mathematics

MDPI

Article

Impacts of Thermal Radiation and Heat Consumption/Generation on Unsteady MHD Convection Flow of an Oldroyd-B Fluid with Ramped Velocity and Temperature in a Generalized Darcy Medium

Talha Anwar [1], Ilyas Khan [2,*], Poom Kumam [1,3,4,*] and Wiboonsak Watthayu [1]

[1] Department of Mathematics, Faculty of science, King Mongkut's University of Technology Thonburi (KMUTT), 126 Pracha-Uthit Road, Bang Mod, Thrung Khru, Bangkok 10140, Thailand; anwartalha80@gmail.com (T.A.); wiboonsak.wat@kmutt.ac.th (W.W.)

[2] Department of Mathematics, College of Science Al-Zulfi, Majmaah University, Al-Majmaah 11952, Saudi Arabia

[3] KMUTT Fixed Point Research Laboratory, Room SCL 802 Fixed Point Laboratory, Science Laboratory Building, Department of Mathematics, Faculty of Science, King Mongkut's University of Technology Thonburi (KMUTT), Bangkok 10140, Thailand

[4] Department of Medical Research, China Medical University Hospital, China Medical University, Taichung 40402, Taiwan

* Correspondence: i.said@mu.edu.sa (I.K.); poom.kum@kmutt.ac.th (P.K.)

Received: 18 December 2019; Accepted: 27 December 2019; Published: 15 January 2020



Abstract: This article analyzes the time-dependent magnetohydrodynamic flow of Oldroyed-B fluid in the presence of heat consumption/generation and thermal radiation. The flow is restricted to a vertical infinite plate saturated in porous material along with ramp wall velocity and ramp wall temperature conditions. This flow also incorporates the generalized Darcy's law. In this paper, accurate equation of velocity field is presented first and then solutions of mass and energy equation are derived in Laplace domain. Real-time domain solutions are obtained by tackling the complexity of Laplace domain expressions through numerical Laplace inversion. Skin friction coefficient and Nusselt number are also calculated. A comparison for ramp wall temperature condition and isothermal temperature condition is also drawn to investigate the difference. A graphical study is conducted to analyze the influence of parameters on fluid flow and heat transfer. It is found that radiation parameter and heat generation elevate the energy profile, while flow is accelerated by increasing the retardation time and porosity parameter and an opposite behavior is noted for increasing relaxation time and magnetic parameter. Furthermore, heat transfer rate is higher for increasing Prandtl number and velocity on plate decreases with increase in relaxation time λ_1.

Keywords: heat consumption; laplace transform; ramp wall; MHD; corrected model; Oldroyd-B fluid

1. Introduction

In emerging and modern technologies, non-Newtonian fluids are gathering attraction due to their high practical significance. Non-Newtonian fluids involve honey, paints, toothpaste, polymer solutions, and greases. In modern days, flow of such fluids together with magnetohydrodynamic (MHD) having free and forced convection are of great use in energy generator purification of mineral oil and power generators. Moving forward, the addition of thermal radiation to such flows has important affects in the mechanisms of aerosol technology, solar collectors, and high temperature

polymeric mixtures, which act at high and medium temperatures [1]. Hydrologists and engineers investigated the flows of fluid in porous materials ranging from fused Pyrex glass to sand packs to anticipate their behaviors in different kinds of reservoirs [2]. Incorporation of heat source or sink to magnetohydrodynamics (MHD) convective fluid has strong usage in welding mechanics and thermal engineering [3,4]. Oldroyd-B fluid lies in the category of non-Newtonian fluids and is completely capable of presenting viscoelastic fluids [5]. We considered this model in this work due to its simplicity, vastness, and complete resemblances with the fluids showing viscous and elastic profiles simultaneously. This model is an extension of the Maxwell model and the viscous model. Moreover, in a special case when viscosity of the solvent vanishes, it reduces to Upper Convected Maxwell fluid. Further details of these models can be approached in References [6–8].

In the literature, there is a dearth of articles when it comes to dealing with flows subjected to ramp wall temperature and ramp wall velocity conditions despite valuable physical significance. One of the main possibilities is the handling of complex resulted expressions. These combined wall conditions have significant applications like diagnoses of cardiovascular diseases using treadmil testing or ergometers. Analysis of blood vessel functioning and diagnoses of heart diseases also depend upon ramp wall velocity conditions. To cure cancer cells, a therapy based on ramp wall conditions is utilized as it has negligible side effects on the human body [9]. To further improve the cure of cancer, different types of boundary conditions were presented by Kundu [9]. More applications of ramped conditions can be studied in the contribution of Schetz [10], Hayday [11], and Malhotra [12].

The idea of simultaneous ramped conditions was proposed by Ahmed and Dutta [13] to study the flow passing an instinctively infinite vertical plate. Mass and heat transfer phenomenons were studied by Seth et al. for ramp temperature conditions in case of moving vertical plates [14–16]. In recent times, Chandran et al. studied the effect of ramp temperature condition on mixed convection fluid flow [17]. A study is conducted by Narahari et al. to analyze the fluid motion for infinite vertical plate with wall heating [18]. An extension of Khan's [19] work on MHD flow of Jeffery fluid was provided by Zin et al. [20] for ramp wall temperature condition. Further, this work was given an extension by Maqbool et al. for simultaneous ramp wall conditions [21]. More applications of ramped conditions can be found in the work of Myers et al. [22] and Bruce [23].

On the basis of such strong motivation, we have considered the free convection flow inculcating thermal radiative effects along MHD. Moreover, heat suction/injection is also introduced to the flow with the existence of a porous medium. The ramp velocity and ramp temperature conditions are considered at the wall. Laplace transformation is implemented to reach the solutions.

2. Mathematical Modeling

The subsequent equations [24,25] describing unsteady, incompressible, and MHD motion of Oldroyd-B fluid over an infinite vertical plate are provided under Boussinesq's approximations [26] as

$$\nabla \cdot \mathbf{V} = 0, \tag{1}$$

$$\rho \left[\frac{\partial \mathbf{V}}{\partial t} + (\mathbf{V}.\nabla)\mathbf{V} \right] = \mathrm{div}\mathbf{T} + \mathbf{J} \times \mathbf{B} + \mathbf{g}\rho\beta(T - T_\infty) + \mathbf{r}. \tag{2}$$

where ρ, $\mathbf{r}$, $\mathbf{J}$, $\mathbf{B}$, g, β, t, and T represent fluid density, Darcy's resistence, current density, total magnetic field, gravitational acceleration, thermal volume expansion, time, and temperature of fluid, respectively. Moreover, velocity $\mathbf{V}$, accounting for one-dimensional and unidirectional flow, and the Cauchy stress tensor $\mathbf{T}$ are defined as

$$\mathbf{V} = [u(y,t), 0, 0], \tag{3}$$

$$\mathbf{T} = -\mathscr{P}\mathbf{I} + \mathbf{S}. \tag{4}$$

where $\mathbf{S}$ and $-\mathscr{P}\mathbf{I}$ denote the extra stress tensor and indeterminate stress tensor, respectively. Moreover, $\mathbf{S}$ holds the following relation:

$$\mu\left(1+\lambda_r\frac{D}{Dt}\right)\mathbf{A}_1=\mathbf{S}\left(1+\lambda\frac{D}{Dt}\right), \tag{5}$$

where μ refers to dynamic viscosity of fluid. λ_r and λ refer to retardation and relaxation time, respectively. Additionally, material time derivative $\frac{D}{Dt}$ and Rivlin–Ericksen tensor $\mathbf{A}_1$ are defined as

$$\frac{D\mathbf{S}}{Dt}=\frac{\partial\mathbf{S}}{\partial t}+u\frac{\partial\mathbf{S}}{\partial x}+v\frac{\partial\mathbf{S}}{\partial y}+w\frac{\partial\mathbf{S}}{\partial z}, \tag{6}$$

$$\mathbf{A}_1=\nabla\mathbf{V}+(\nabla\mathbf{V})^T=\begin{pmatrix}0 & u_y\\ u_y & 0\end{pmatrix}. \tag{7}$$

where x, y, z and u, v, w are space variables and velocity components. For Oldroyd-B fluid, modified Darcy's law is defined as

$$-\frac{\mu\phi}{k}\left(1+\lambda_r\frac{\partial}{\partial t}\right)\mathbf{V}=\left(1+\lambda\frac{\partial}{\partial t}\right)\mathbf{r}, \tag{8}$$

where ϕ and k are porosity and permeability of the porous medium. The equations of Maxwell are given as

$$\mathrm{div}\mathbf{B}=0,\quad \mathrm{curl}\mathbf{B}=\boldsymbol{\mu}_m\mathbf{J},\quad \mathrm{curl}\mathbf{E}=-\frac{\partial\mathbf{B}}{\partial \mathrm{t}}, \tag{9}$$

$$\mathbf{J}\times\mathbf{B}=-(\boldsymbol{\sigma}\boldsymbol{B}_0^2\boldsymbol{u},\mathbf{0},\mathbf{0}). \tag{10}$$

where $\boldsymbol{\mu}_m$, $\boldsymbol{\sigma}$, and $\mathbf{E}$ refer to magnetic permeability, electrical conductivity, and electric field, respectively. The total magnetic field is given as $\mathbf{B}=B_0+b_0$. Here, B_0 denotes the magnetic field applied and b_0 denotes the magnetic field induced.

In the presence of Equations (3)–(8), a deduced form of Equation (2) can be presented as

$$\rho\frac{\partial u}{\partial t}=\rho g\beta(T-T_\infty)+\mathbf{r}_x+(\mathbf{J}\times\mathbf{B})_x+\frac{\partial S_{xy}}{\partial y}, \tag{11}$$

Using Maxwell's equations and modified Darcy's law in the above equation and multiplying it by $(1+\lambda\partial_t)$, we obtain the following form:

$$\begin{aligned}(1+\lambda\partial_t)\rho\frac{\partial u}{\partial t}&=(1+\lambda\partial_t)\rho g\beta(T-T_\infty)-(1+\lambda_r\partial_t)\frac{\mu\phi}{k}u\\&\quad-(1+\lambda\partial_t)\sigma B_0^2u+(1+\lambda\partial_t)\frac{\partial S_{xy}}{\partial y},\end{aligned} \tag{12}$$

Using relation $(1+\lambda\partial_t)S_{xy}=\mu(1+\lambda_r\partial_t)u_y$ in the above equation and rearranging the resulting equation in some fascinating manner, the correct presentation of velocity equation is obtained as

$$\rho(1+\lambda\frac{\partial}{\partial t})\frac{\partial u}{\partial t} = \mu(1+\lambda_r\frac{\partial}{\partial t})\frac{\partial^2 u}{\partial y^2} + \rho g\beta(1+\lambda\frac{\partial}{\partial t})(T-T_\infty) - \sigma B_0^2(1+\lambda\frac{\partial}{\partial t})u - \frac{\mu\phi}{k}(1+\lambda_r\frac{\partial}{\partial t})u. \quad (13)$$

However, in the work of Mazhar et al. [27], the term $1+\lambda\frac{\partial}{\partial t}$ is missing with the coefficient of thermal expansion pointing out the deficiency of their model. The geometrical presentation of considered model is provided in Figure 1.

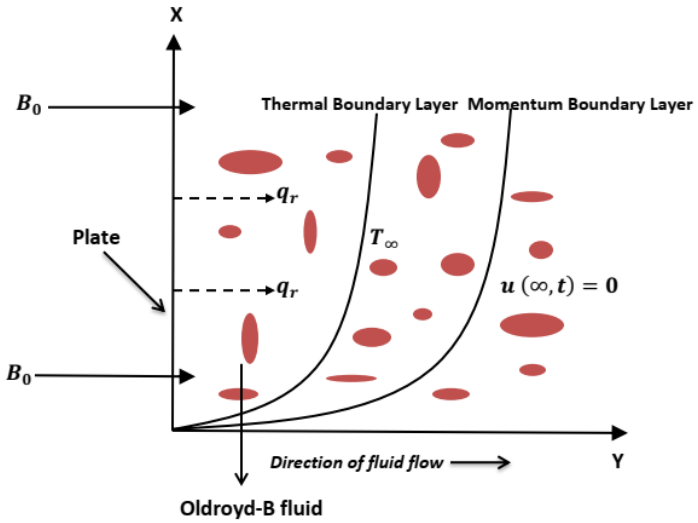

Figure 1. Geometrical presentation of flow.

The governing equations for flow and energy under the assumptions of Boussinesq's approximation and small Reynolds number are provided as

$$(1+\lambda\frac{\partial}{\partial t})\frac{\partial u}{\partial t} = \nu(1+\lambda_r\frac{\partial}{\partial t})\frac{\partial^2 u}{\partial y^2} + g\beta(1+\lambda\frac{\partial}{\partial t})(T-T_\infty) - \frac{\sigma B_0^2}{\rho}(1+\lambda\frac{\partial}{\partial t})u - \frac{\nu\phi}{k}(1+\lambda_r\frac{\partial}{\partial t})u, \quad (14)$$

$$\rho c_p\frac{\partial T}{\partial t} = k\frac{\partial^2 T}{\partial y^2} - \frac{\partial q_r}{\partial y} + Q_0(T-T_\infty), \quad (15)$$

where $\rho c_p, k, q_r$, and Q_0 refer to heat capacitance, thermal conductivity, radiative heat flux, and heat generation/absorption constant.

The associated initial and boundary conditions are defined as

$$u(y,0) = 0, \quad T(y,0) = T_\infty,$$
$$y \geq 0: \quad u_t(y,0) = 0, \quad u_y(y,0) = 0, \quad (16)$$
$$t > 0: \quad u(y,t) \to 0, \quad T(y,t) \to T_\infty, \quad \text{for} \quad y \to \infty, \quad (17)$$
$$u(0,t) = \begin{cases} u_0\frac{t}{t_0} & 0 < t \leq t_0 \\ u_0 & t > t_0 \end{cases}$$
$$T(0,t) = \begin{cases} T_\infty + (T_w - T_\infty)\frac{t}{t_0} & 0 < t \leq t_0 \\ T_w & t > t_0 \end{cases} \quad (18)$$

The radiation heat flux, after using Rosseland approximation comes out to be [28]

$$q_r = -\frac{4\sigma_1 \partial T^4}{3k_1 \partial y}. \tag{19}$$

where the Stafan–Boltzman constant and adsorption coefficient are represented by σ_1 and k_1, respectively. The term q_r can be linearized by expansion of T^4 using Taylor series about T_∞, keeping the supposition in mind that temperature differences are small enough to neglect the higher-order terms. After normalizing, T^4 comes out to be $T^4 \approx 4T_\infty^3 T - 3T_\infty^4$.

Using this linearization in Equation (15) results in

$$\rho c_p \frac{\partial T}{\partial t} = k\left(1 + \frac{16\sigma_1 T_\infty^3}{3k_1 k}\right)\frac{\partial^2 T}{\partial y^2} + Q_0(T - T_\infty). \tag{20}$$

For the sake of braveity, dimensionless terms are defined as

$$u^* = \frac{u}{u_0}, \quad \eta = \frac{yu_0}{\nu}, \quad \tau = \frac{tu_0^2}{\nu}, \quad \tau_0 = \frac{\nu}{u_0^2}, \quad \theta = \frac{T - T_\infty}{T_w - T_\infty}. \tag{21}$$

Introducing the above terms in the equations of flow and energy and dropping the $*$ for convenience, they take the following form:

$$\left(a_1 + \lambda_1 \frac{\partial}{\partial \tau}\right)\frac{\partial u}{\partial \tau} = \left(1 + \lambda_2 \frac{\partial}{\partial \tau}\right)\frac{\partial^2 u}{\partial \eta^2} - b_1 u + Gr\left(1 + \lambda_1 \frac{\partial}{\partial \tau}\right)\theta, \tag{22}$$

$$\frac{\partial \theta}{\partial \tau} = \left(\frac{1 + Nr}{Pr}\right)\frac{\partial^2 \theta}{\partial \eta^2} + Q\theta. \tag{23}$$

where dimensionless parameters are defined as

$$\begin{aligned} Gr &= \frac{g\beta\nu(T_w - T_\infty)}{u_0^3}, \quad Nr = \frac{16\sigma_1 T_\infty^3}{3kk_1}, \quad M = \frac{\sigma B_0^2 \nu}{\rho u_0^2}, \\ Pr &= \frac{\mu c_p}{k}, \quad b_1 = M + \frac{1}{K}, \quad \lambda_1 = \frac{\lambda u_0^2}{\nu}, \quad \lambda_2 = \frac{\lambda_r u_0^2}{\nu}, \\ \frac{1}{K} &= \frac{\phi \nu^2}{k u_0^2}, \quad Q = \frac{\nu Q_0}{\rho c_p u_0^2}, \quad a_1 = 1 + \lambda_1 M + \frac{\lambda_2}{K}, \end{aligned} \tag{24}$$

The initial and boundary conditions in dimensionless form can be presented as

$$u(\eta, 0) = 0, \quad \theta(\eta, 0) = 0, \tag{25}$$

$$\eta \geq 0: \quad u_\tau(\eta, 0) = 0, \quad u_\eta(\eta, 0) = 0,$$

$$\tau > 0: \quad u(\eta, \tau) \to 0, \quad \theta(\eta, \tau) \to 0 \quad \text{when} \quad \eta \to \infty, \tag{26}$$

$$u(0, \tau) = \theta(0, \tau) = \begin{cases} \tau & 0 < \tau \leq 1 \\ 1 & \tau > 1, \end{cases} \tag{27}$$

3. Analytical Solutions

To generate the solution of this problem, Laplace transform [29] is a convenient tool due to its effective applicability for nonuniform boundary conditions. Other convenient methods like Adomian decomposition, Homotopy analysis method, perturbation method, and separation of variables do not

serve the purpose here due to complicated boundary conditions. We formulate the Laplace transform pair for the sake of the results of current problem as an integral of the following form:

$$\bar{R}(\eta, q) = \int_0^\infty e^{-q\tau} R(\eta, \tau) d\tau = \mathcal{L}[R](\tau), \qquad \tau \geq 0, \tag{28}$$

where $R \in \{u, \theta\}$. The above integral is convergent for $Re(q) > \gamma_0$ where $q = \Psi + j\Omega$, γ_o is a real number, and $j = \sqrt{-1}$. Transformation of the Laplace domain solutions back to the original time domain can be performed as

$$R(\eta, \tau) = \frac{1}{2\pi j} \int_{BR} e^{q\tau} \bar{R}(\eta, q) dq = \mathcal{L}^{-1}[\bar{R}](q), \tag{29}$$

Implementation of Laplace transform on mass and energy equations and putting $a_1 = \frac{1+Nr}{Pr}$ in the energy equation yields

$$q\bar{\theta} = a_1 \frac{\partial^2 \bar{\theta}}{\partial \eta^2} + Q\bar{\theta}, \tag{30}$$

$$\frac{\partial^2 \bar{u}}{\partial \eta^2} - \left(\frac{a_1 q + q^2 \lambda_1 + b_1}{1 + \lambda_2 q} \right) \bar{u} = -Gr \left(\frac{1 + \lambda_1 q}{1 + \lambda_2 q} \right) \bar{\theta}, \tag{31}$$

Application of Laplace transform on initial and boundary condition responds as

$$\bar{u}(\eta, 0) = 0, \quad \bar{\theta}(\eta, 0) = 0, \tag{32}$$

$$\bar{u}(\eta, q) \to 0, \quad \bar{\theta}(\eta, q) \to 0 \quad \text{for} \quad \eta \to \infty, \tag{33}$$

$$\bar{u}(0, q) = \bar{\theta}(0, q) = \frac{1 - e^{-q}}{q^2}. \tag{34}$$

Solution of the energy equation in Equation (30) in Laplace domain subjected to the boundary conditions in Equations (33) and (34) is given as

$$\bar{\theta}(\eta, q) = \left(\frac{1 - e^{-q}}{q^2} \right) e^{-\sqrt{\alpha(q-Q)}\eta}. \tag{35}$$

Plugging in the value of $\bar{\theta}$ in mass in Equation (31) implies

$$\frac{\partial^2 \bar{u}}{\partial \eta^2} - \left(\frac{a_1 q + q^2 \lambda_1 + b_1}{1 + \lambda_2 q} \right) \bar{u} = -Gr \left(\frac{1 + \lambda_1 q}{1 + \lambda_2 q} \right) \left(\frac{1 - e^{-q}}{q^2} \right) e^{-\sqrt{\alpha(q-Q)}\eta}. \tag{36}$$

The solution of the above equation subjected to boundary conditions is given as

$$\bar{u}(\eta, q) = \left(\frac{1 - e^{-q}}{q^2} \right) \bar{H}(\eta, q),$$

$$\bar{H}(\eta, q) = e^{-\sqrt{\frac{a_1 q + q^2 \lambda_1 + b_1}{1 + \lambda_2 q}}\eta} + \frac{Gr(1 + \lambda_1 q) e^{-\sqrt{\frac{a_1 q + q^2 \lambda_1 + b_1}{1 + \lambda_2 q}}\eta}}{(\lambda_2 \alpha - \lambda_1)[(q - m_1)^2 - m_2^2]} - \frac{Gr(1 + \lambda_1 q) e^{-\sqrt{\alpha(q-Q)}\eta}}{(\lambda_2 \alpha - \lambda_1)[(q - m_1)^2 - m_2^2]}, \tag{37}$$

where

$$m_1 = \frac{a_1 + \lambda_2 \alpha Q - \alpha}{2(\lambda_2 \alpha - \lambda_1)}, \quad m_2 = \sqrt{\left(\frac{a_1 + \lambda_2 \alpha Q - \alpha}{2(\lambda_2 \alpha - \lambda_1)} \right)^2 + \frac{b_1 + \alpha Q}{\lambda_2 \alpha - \lambda_1}}. \tag{38}$$

Since the mass and energy fields contain the complex combinations of Laplace parameter q, numerical inversion named as Durbin method [30] is applied to deduce the solutions in a real-time domain τ.

The expressions for Nusselt number Nu and skin friction τ_w are given as

$$Nu = -\frac{\partial \theta}{\partial \eta}(0,\tau), \tag{39}$$

$$Nu = \mathcal{L}^{-1}\left[\sqrt{\alpha(q-Q)}\left(\frac{1-e^{-q}}{q^2}\right)\right], \tag{40}$$

$$\tau_w = \frac{\mu}{1+\lambda_1\partial_\tau}(1+\lambda_2\partial_\tau)\frac{\partial u}{\partial \eta}(0,\tau), \tag{41}$$

where

$$\frac{\partial u}{\partial \eta}(0,\tau) = \frac{\partial H}{\partial \eta}(0,\tau) + \frac{\partial H(0,\tau-1)F(\tau-1)}{\partial \eta}. \tag{42}$$

4. Special Cases

This section deals with some special cases of the current work.

4.1. Case 1

The solution of viscous fluid with ramp wall temperature can be fetched when $\lambda_1 = 0$ and $\lambda_2 = 0$ [31].

$$\theta(\eta,q) = \mathcal{L}^{-1}\left[\left(\frac{1-e^{-q}}{q^2}\right)e^{-\sqrt{\alpha(q-Q)}\eta}\right], \tag{43}$$

$$u(\eta,\tau) = \mathcal{L}^{-1}\left[\frac{1}{q}e^{-\sqrt{q+b_1}\eta} + \left(\frac{Gr}{\alpha(q-Q)-(q+b_1)}\frac{1-e^{-q}}{q^2}\right)(e^{-\sqrt{q+b_1}\eta} - e^{-\sqrt{\alpha(q-Q)}\eta})\right]. \tag{44}$$

4.2. Case 2

The Maxwell fluid flow profiles can be derived when $\lambda_2 = 0$ [32].

4.3. Case 3

The simultaneous ramp wall conditional solutions of Oldroyd-B fluid can be deduced when Nr, $Q \to 0$.

$$\theta(\eta,\tau) = \mathcal{L}^{-1}\left[\frac{1-e^{-q}}{q^2}e^{-\sqrt{Prq}\eta}\right], \tag{45}$$

$$u(\eta,\tau) = \mathcal{L}^{-1}\left[\left(\frac{1-e^{-q}}{q^2}\right)\bar{H}(\eta,q)\right]. \tag{46}$$

where

$$\bar{H}(\eta,q) = e^{-\sqrt{\frac{a_1q+q^2\lambda_1+b_1}{1+\lambda_2q}}\eta} + \frac{Gr(1+\lambda_1q)e^{-\sqrt{\frac{a_1q+q^2\lambda_1+b_1}{1+\lambda_2q}}\eta}}{(\lambda_2Pr-\lambda_1)[(q-m_1)^2-m_2^2]} - \frac{Gr(1+\lambda_1q)e^{-\sqrt{Prq}\eta}}{(\lambda_2Pr-\lambda_1)[(q-m_1)^2-m_2^2]},$$

$$m_1 = \frac{a_1-Pr}{2(\lambda_2Pr-\lambda_1)}, \quad m_2 = \sqrt{\left(\frac{a_1-Pr}{2(\lambda_2Pr-\lambda_1)}\right)^2 + \frac{b_1}{\lambda_2Pr-\lambda_1}}. \tag{47}$$

4.4. Case 4

The mass and energy solutions of Oldroyd-B fluid for constant boundary conditions can be deduced as

$$\theta(\eta,\tau) = e^{-\eta i\sqrt{\alpha Q}}\,\mathrm{erfc}\left(\frac{\eta\sqrt{Q}}{2\sqrt{\tau}} - i\sqrt{Q\tau}\right) + e^{\eta i\sqrt{\alpha Q}}\,\mathrm{erfc}\left(\frac{\eta\sqrt{Q}}{2\sqrt{\tau}} + i\sqrt{Q\tau}\right), \tag{48}$$

$$u(\eta,\tau) = \mathcal{L}^{-1}\left[\left(\frac{1-e^{-q}}{q}\right)\bar{H}(\eta,q)\right], \tag{49}$$

where

$$\bar{H}(\eta,q) = e^{-\sqrt{\frac{a_1q+q^2\lambda_1+b_1}{1+\lambda_2 q}}\eta} + \frac{Gr(1+\lambda_1 q)e^{-\sqrt{\frac{a_1q+q^2\lambda_1+b_1}{1+\lambda_2 q}}\eta}}{(\lambda_2\alpha-\lambda_1)[(q-m_1)^2-m_2^2]} - \frac{Gr(1+\lambda_1 q)e^{-\sqrt{\alpha(q-Q)}\eta}}{(\lambda_2\alpha-\lambda_1)[(q-m_1)^2-m_2^2]}. \tag{50}$$

5. Parametric Study

The meaningful role of several associated parameters on the mass and energy boundary layer is interpreted with the help of graphs in this section. These graphs of mass and energy profiles have two types of solution: (1) the solution with simultaneous ramp wall conditions and denoted by solid lines and (2) the solution with ramp wall velocity and isothermal temperature conditions and denoted by dashed lines.

First of all, a velocity profile comparison of the present work and the solution of the corrected model of Reference [27] is graphed in Figure 2, and a good agreement is observed in both solutions in the absence of heat consumption/generation and radiation effects. Figure 3 indicates that an increase in Gr values provides enhancement in the momentum boundary layer. It is supported by the physical fact that Gr is the fraction of buoyancy and viscous forces. An increase in Gr means that the buoyancy force gets stronger near the plate, that it overcomes the viscous force, and that the fluid gets accelerated. It is observed that the momentum boundary layer has more thickness in the case of isothermal temperature as compared to ramp temperature. Figure 4 presents the mass distribution under the influence of a magnetic parameter. It is witnessed that an increase in the magnetic parameter decreases the momentum boundary layer. The reason is the strong Lorentz force induced due to magnetic field. This strong Lorentz force acts as a resistance and decreases the velocity of fluid. Similar profiles are observed for ramped temperature and isothermal temperature. In Figure 5, the effect of changes in porosity parameter K is illustrated for isothermal and ramped temperature. It is observed that velocity for isothermal temperature is greater as compared to ramped temperature. Furthermore, It is also noticed that an increase in porosity reduces the friction of porous material which in turn increases the momentum development of the regime and, as a result, the velocity profile is enhanced. Figure 6 covers the influence of relaxation time λ_1 on velocity behavior. It is witnessed that the increasing variation of λ_1 reduces the thickness of momentum boundary layer which results in deceleration of the fluid. As a relaxation time increment implies that the fluid will take extra time to calm, it readily justifies the decrease in velocity. Afterwards, a comparison analysis describes that the ramped condition velocity is higher than the isothermal velocity. The role of Pr on the velocity curve is graphed in Figure 7. It is found that fluids having larger Pr values have lower velocity. The physical phenomenon behind this behavior is the increment in viscous force. It means the dragging force gets stronger with increase in Pr and results in retardation of fluid velocity. The contribution of Nr is shown in Figure 8 for both isothermal and ramped plates. It is found that the enhancement in Nr increases the thickness of the momentum boundary layer. This enhancement is physically justified by the high rate of transfer of energy when Nr is increased. This higher energy transfer rate weakens the bonds between fluid particles which results in the form of weaker resistance, and eventually, the fluid gets accelerated. It is also revealed that the velocity profile of the isothermal plate is higher than that of the ramped

plate. Figure 9 reveals the impact of retardation time λ_2 on velocity solution. It is observed that both ramped and isothermal solutions get higher profiles in the case of increasing retardation time. This is justified by the fact that an increase in λ_2 decreases the effect of friction. Therefore, for large values of λ_2, the thickness of the momentum boundary layer increases. Figure 10 depicts that enlargement in time τ raises the velocity profiles of both ramped and isothermal wall.

Figure 11 shows a good agreement between the present work and the result of Mazhar et al. [27] when radiation and heat consumption/generation are removed from the thermal system. The function of Pr on temperature profiles is given in Figure 12. It is witnessed that temperature decreases for larger Pr values. The physical reason is the reduction of thermal conductivity. It means the fluid receives small amounts of heat when Pr increases. For lower Pr values, the fluid has higher thermal conductivity, and for large Pr values, the fluid faces more resistance. Moreover, temperature boundary layer thickness is observed to be greater in the case of the isothermal plate. Figure 13 sketches the significance of variating Nr on temperature curves. An elevation in temperature profile is witnessed for increasing Nr values. Physically, k^* reduces due to the enhancement in divergence of radiative heat flux $\frac{\partial q_r}{\partial y}$. This leads to increases in the amount of radiative heat transfer to the fluid, and ultimately, the temperature of the fluid gets elevated. The influence of installed heat consumption and generation is illustrated in Figure 14. In the graph, negative values of Q are associated with heat consumption and positive values of Q refer to heat generation. Physically, an increase in negative value of Q refers to more consumption of heat and eventually a drop of temperature, as graphed in Figure 14. Similarly, an increase in positive values of Q refers to more heat generation and eventually a raise in temperature. Additionally, a temperature profile for ramped wall is observed lower as compared to the isothermal wall. Figure 15 describes that temperature gets elevated with the extension of time τ.

Figures 16 and 17 showcase the exact inverse behavior of rate of heat transfer for increasing Pr and Nr values. An effective behavior is witnessed; for increasing Pr, Nusselt number gets elevated very rapidly for $\tau < 1$, but after this, it starts decreasing. On the other hand, increasing Nr leads to a decrease in the rate of heat transfer. As noticed for Pr, the Nusselt number for Nr increases for $\tau < 1$ and, then, it starts decreasing. Additionally, for the case of the isothermal plate, only one kind of behavior is observed. In Figure 18, the role of heat consumption and generation in the transfer of heat is presented. It is noticed that, when large amounts of heat are consumed $(Q < 0)$, the heat transfer rate from plate to fluid has a higher magnitude. Oppositely, when more heat is generated $(Q > 0)$, the magnitude of heat transfer rate decreases.

Significance of relaxation and retardation time (λ_1, λ_2) in the behavior of shear stress is graphed in Figure 19. It is spotted that the magnitude of skin friction decreases for $\tau < 1$ as a result of increasing λ_1, but after that, it starts increasing. This behavior is justified by the fact that small viscosity brings a significant decrease in skin friction. Contrarily, skin friction is elevated by the higher values of retardation time λ_2.

The numerical variation in heat transfer rate and skin friction is tabulated for influencing parameters in Tables 1 and 2. Table 1 shows that that Nusselt number gets elevated with an increase in τ and Pr. An interesting observation is made here; for ramp wall conditions, heat transfer rate initially increases for $0 < \tau < 1$ and then faces a decay after $\tau > 1$. Moreover, heat transfer rate decreases with enhancement in Nr and Q. Table 2 presents that shear stress enhances with an increase in τ, Gr, and K and that an inverse behavior is observed for increasing M and λ_2. In the tables, bold values are presented for the particular parameters to show how the results are changing with those parameters.

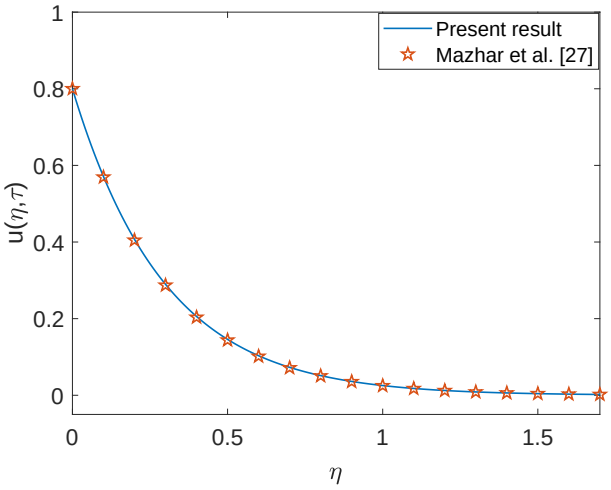

Figure 2. Velocity comparison.

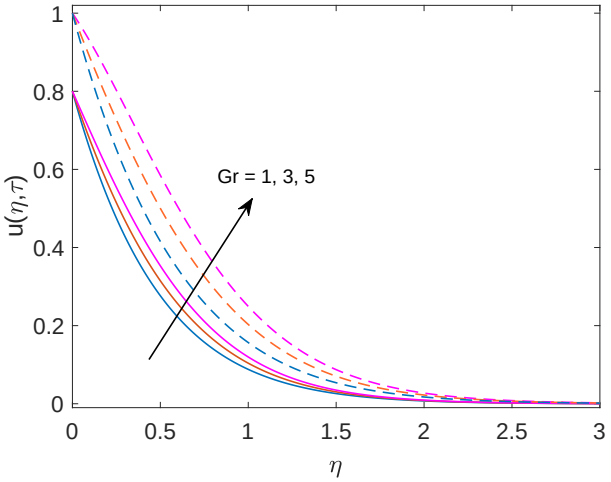

Figure 3. Effect of different values of Gr.

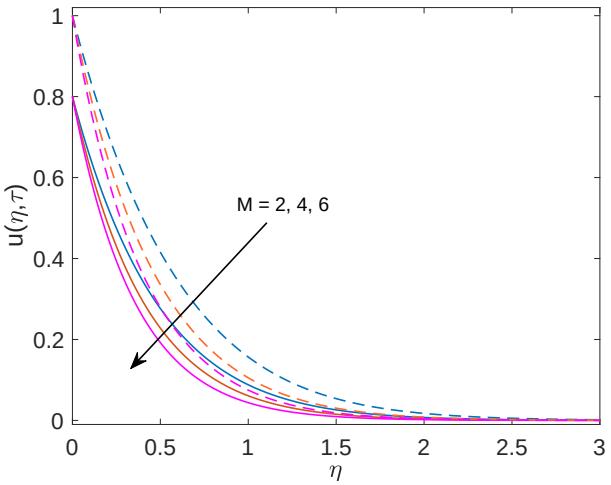

Figure 4. Effect of different values of M.

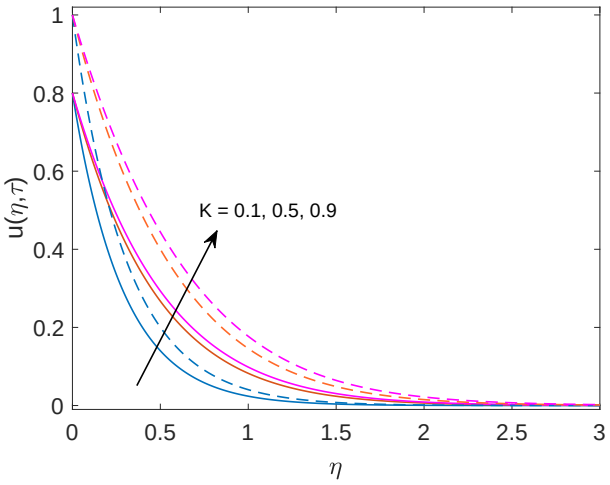

Figure 5. Effect of different values of K.

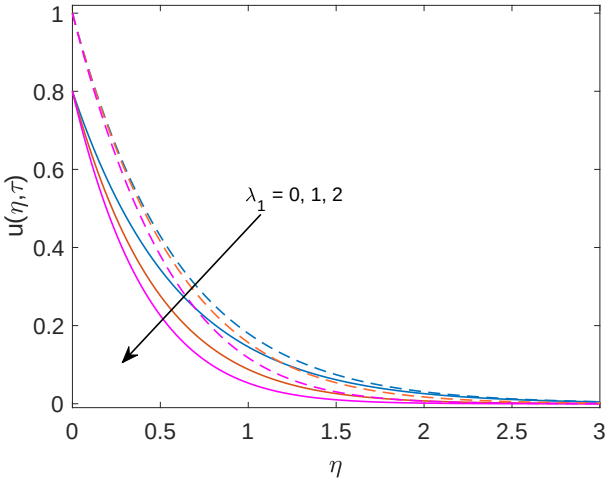

Figure 6. Effect of different values of λ_1.

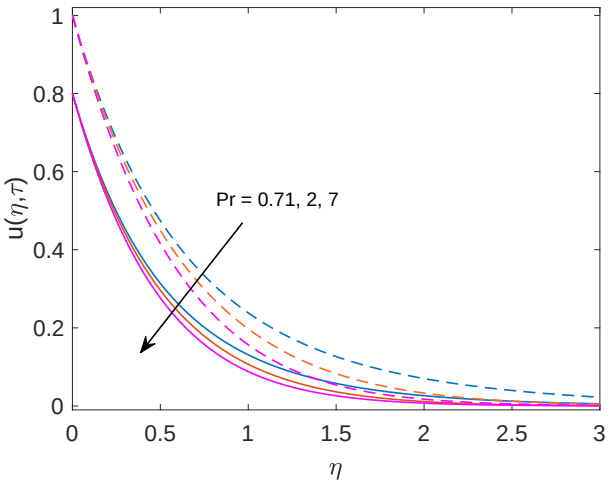

Figure 7. Effect of different values of Pr.

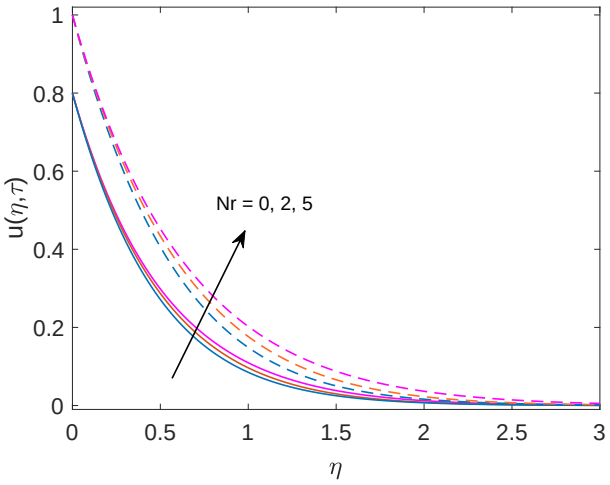

Figure 8. Effect of different values of Nr.

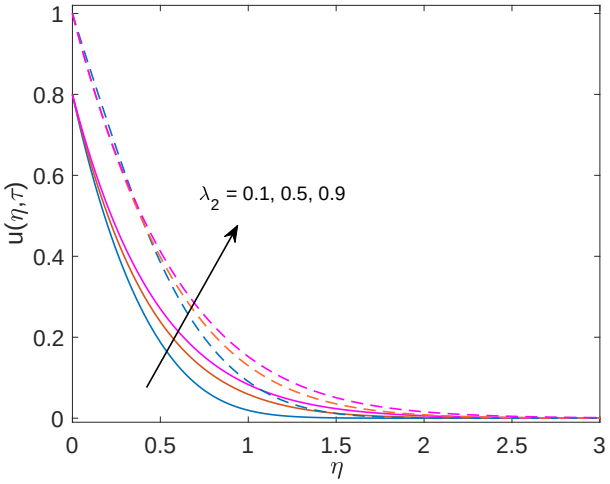

Figure 9. Effect of different values of λ_2.

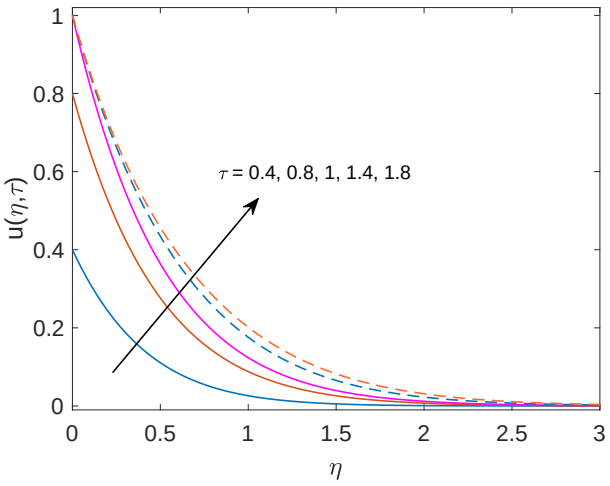

Figure 10. Effect of different values of τ.

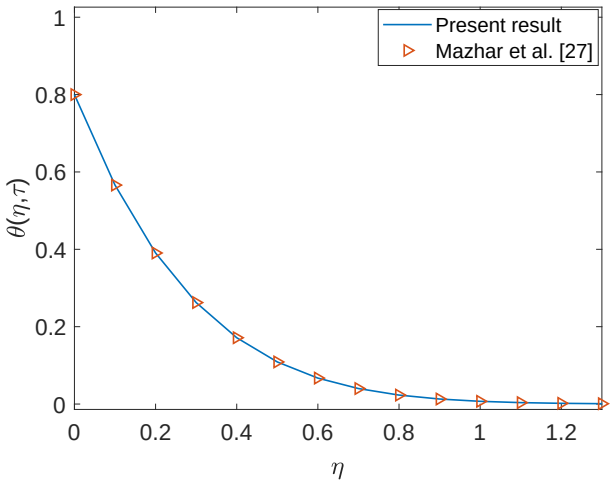

Figure 11. Temperature comparison.

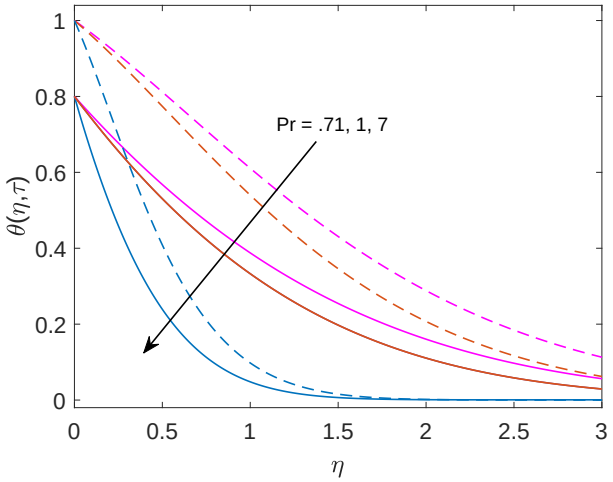

Figure 12. Effect of different values of Pr.

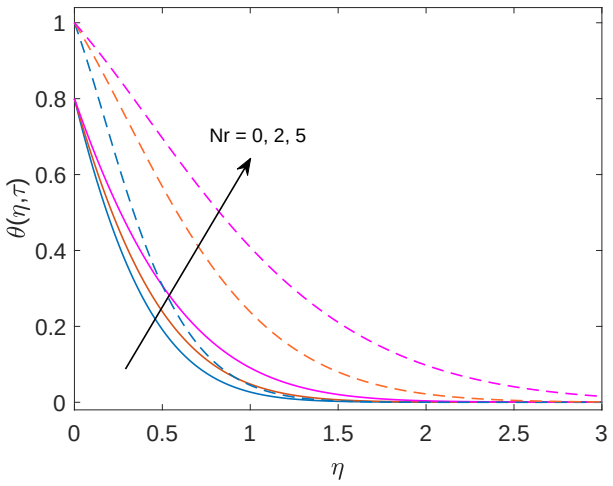

Figure 13. Effect of different values of Nr.

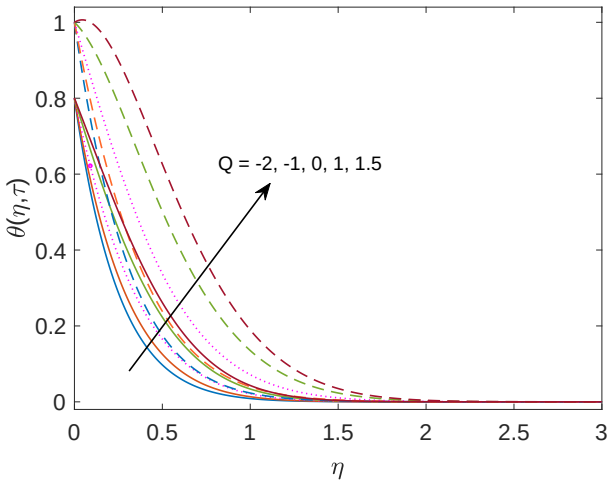

Figure 14. Effect of different values of Q.

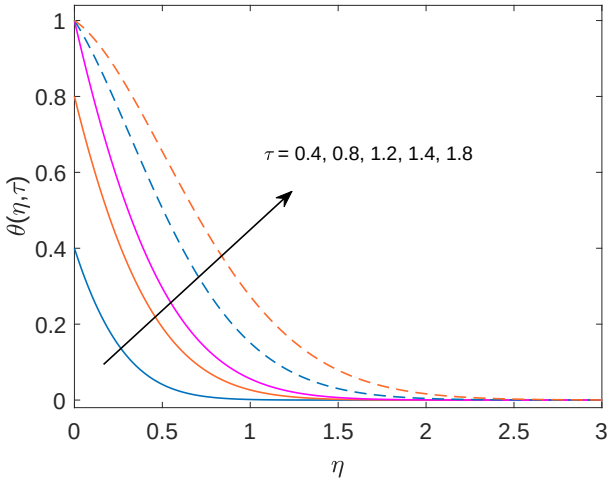

Figure 15. Effect of different values of τ.

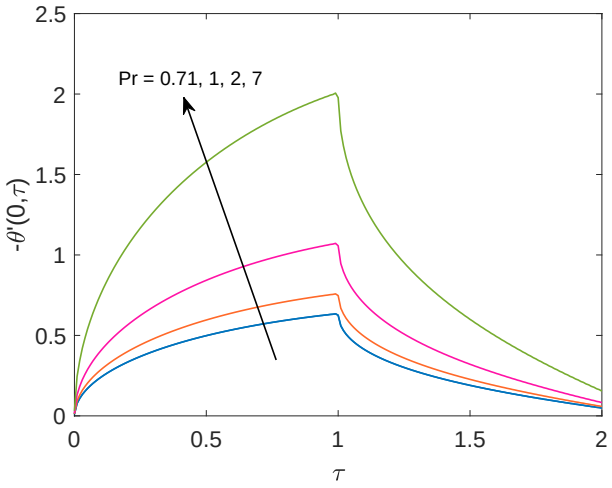

Figure 16. Nusselt number for different values of Pr.

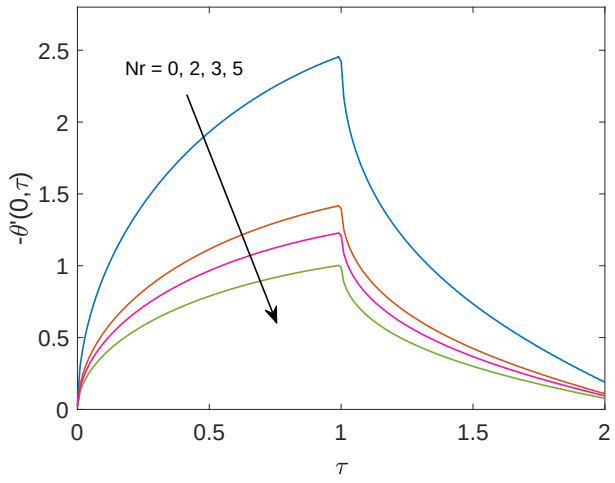

Figure 17. Nusselt number for different values of Nr.

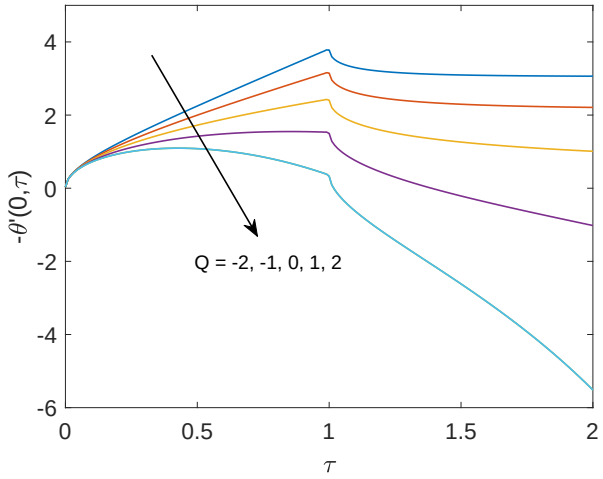

Figure 18. Nusselt number for different values of Q.

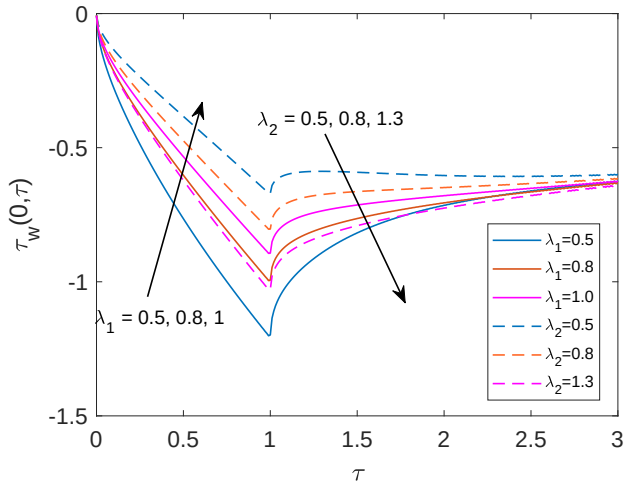

Figure 19. Skin friction for different values of λ_1 and λ_2.

Table 1. Varaition of Nusselt number for different values of parameters.

τ	Pr	Nr	Q	Nu
0.3	7.0	0.5	0.5	**1.2672**
0.4	7.0	0.5	0.5	**1.4366**
0.5	7.0	0.5	0.5	**1.5761**
0.5	**0.71**	0.5	0.5	**0.4984**
0.5	**2.0**	0.5	0.5	**0.8425**
0.5	**7.0**	0.5	0.5	**1.5761**
0.5	7.0	**0**	0.5	**1.9304**
0.5	7.0	**2**	0.5	**1.1145**
0.5	7.0	**3**	0.5	**0.9652**
0.5	7.0	0.5	**0**	**1.7235**
0.5	7.0	0.5	**1**	**1.4208**
0.5	7.0	0.5	**2**	**1.0814**

Table 2. Varaition of skin friction for different values of parameters.

τ	M	K	λ_1	λ_2	Gr	τ_w
0.3	2.0	0.5	1.0	1.0	1.0	**−0.4013**
0.4	2.0	0.5	1.0	1.0	1.0	**−0.4941**
0.5	2.0	0.5	1.0	1.0	1.0	**−0.5845**
0.5	**3.0**	0.5	1.0	1.0	1.0	**−0.6320**
0.5	**4.0**	0.5	1.0	1.0	1.0	**−0.6768**
0.5	**5.0**	0.5	1.0	1.0	1.0	**−0.7192**
0.5	2.0	**0.2**	1.0	1.0	1.0	**−0.7192**
0.5	2.0	**0.5**	1.0	1.0	1.0	**−0.5845**
0.5	2.0	**0.9**	1.0	1.0	1.0	**−0.5396**
0.5	2.0	0.5	**0.5**	1.0	1.0	**−0.8244**
0.5	2.0	0.5	**0.8**	1.0	1.0	**−0.6567**
0.5	2.0	0.5	**1.0**	1.0	1.0	**−0.5845**
0.5	2.0	0.5	1.0	**0.5**	1.0	**−0.4252**
0.5	2.0	0.5	1.0	**0.8**	1.0	**−0.5219**
0.5	2.0	0.5	1.0	**1.3**	1.0	**−0.6763**
0.5	2.0	0.5	1.0	1.0	**0.5**	**−0.5845**
0.5	2.0	0.5	1.0	1.0	**0.8**	**−0.5455**
0.5	2.0	0.5	1.0	1.0	**1.3**	**−0.5065**

6. Conclusions

The main focus of this work is to examine the impact of ramp wall velocity and temperature together on time-dependent MHD convective flow of an Oldroyd-B fluid. The model also involves the porous medium, heat consumption/generation, and thermal radiation. During the modeling of flow, deficiency of Reference [27] modeling is removed and the correct equation of velocity is obtained. Laplace transformation is used as a solution finding tool. The simultaneous ramp wall conditions lead to complex combinations of Laplace paramter in solutions. To overcome this situation, numerical Laplace inversion named as Durbin Method is used and solutions are obtained in the original time domain. The behavioral study of mass and energy profiles under associated parameters is conducted and provided through graphs. Moreover, a comparison of ramp wall temperature and isothermal temperature is also obtained for different parameters. Lastly, expressions for shear stress and heat transfer rate are also calculated and the influence of parameters on them is given in the form of tables and graphs.

The important results of this investigation are as follows:

- An elevation in mass profile is seen with the enhancement in Gr, K, λ_2, and t. An increase in magnetic parameter (M) and relaxation time λ_1 leads to lowering of velocity curves.
- Energy boundary layer decreases with elevation in Pr and addition of heat sink to the system. Increases in Nr and t and addition of a heat source increase the energy boundary layer.
- Nusselt number indicates that high values of Pr provide resistance to heat transfer while small values of Pr have greater thermal conductivity. Moreover, the rate of heat transfer from plate to fluid decays with increase in Nr and Q.
- Velocity on the plate decreases with increase in relaxation time λ_1 and behaves oppositely for retardation time λ_2 (skin friction).

Author Contributions: Conceptualization, T.A. and I.K.; methodology, T.A. and I.K.; software, T.A. and W.W.; validation, P.K. and I.K.; formal analysis, P.K. and W.W.; investigation, P.K. and I.K.; resources, P.K.; writing—original draft preparation, T.A.; writing—review and editing, P.K. and I.K.; visualization, P.K. and W.W.; supervision, P.K. and W.W.; project administration, P.K. All authors have read and agreed to the published version of the manuscript.

Funding: Deanship of Scientific Research at Majmaah University for supporting this work under Project Number No. R-1441-55. Petchra Pra Jom Klao Doctoral Scholarship for Ph.D. program of King Mongkut's University of Technology Thonburi (KMUTT) (Grant No. 14/2562) and Theoretical and Computational Science (TaCS) Center.

Acknowledgments: The author (Ilyas Khan) would like to thank Deanship of Scientific Research at Majmaah University for supporting this work under Project Number No. R-1441-55. The authors appreciate the financial support allotted by King Mongkut's University of Technology Thonburi through the "KMUTT 55th Anniversary Commemorative Fund". The first author is supported by the Petchra Pra Jom Klao Doctoral Scholarship Academic for PhD studies at KMUTT. This research is accomplished with the help of Theoretical and Computational Science (TaCS) Center under Computational and Applied Science for Smart Innovation (CLASSIC), Faculty of Science, KMUTT.

Conflicts of Interest: The authors declare no conflict of interest.

References

1. RamReddy, C.; Naveen, P. Analysis of activation energy and thermal radiation on convective flow of a power-law fluid under convective heating and chemical reaction. *Heat Transf. Res.* **2019**, *48*, 2122–2154. [CrossRef]
2. Kucuk, F.; Karakas, M.; Ayestaran, L. Well testing and analysis techniques for layered reservoirs. *SPE Form. Eval.* **1986**, *1*, 342–354. [CrossRef]
3. Hashmi, S. *Comprehensive Materials Processing*; Newnes: Amsterdam, The Netherlands, 2014.
4. Ueda, Y.; Murakawa, H.; Ma, N. *Welding Deformation and Residual Stress Prevention*; Elsevier: Amsterdam, The Netherlands, 2012.
5. Pop, I.; Ingham, D.B. *Convective Heat Transfer: Mathematical and Computational Modelling of Vviscous Fluids and Porous Media*; Elsevier: Amsterdam, The Netherlands, 2001.
6. Oldroyd, J.G. On the formulation of rheological equations of state. *Proc. R. Soc. Lond. Ser. A Math. Phys. Sci.* **1950**, *200*, 523–541.
7. Aman, S.; Khan, I.; Ismail, Z.; Salleh, M.Z.; Al-Mdallal, Q.M. Heat transfer enhancement in free convection flow of CNTs Maxwell nanofluids with four different types of molecular liquids. *Sci. Rep.* **2017**, *7*, 2445. [CrossRef] [PubMed]
8. Heymans, N.; Bauwens, J.C. Fractal rheological models and fractional differential equations for viscoelastic behavior. *Rheol. Acta* **1994**, *33*, 210–219. [CrossRef]
9. Kundu, B. Exact analysis for propagation of heat in a biological tissue subject to different surface conditions for therapeutic applications. *Appl. Math. Comput.* **2016**, *285*, 204–216. [CrossRef]
10. Schetz, J. On the approximate solution of viscous-flow problems. *J. Appl. Mech.* **1963**, *30*, 263–268. [CrossRef]
11. Eichhorn, R. Discussion: "Free Convection From a Vertical Flat Plate with Step Discontinuities in Surface Temperature"(Hayday, AA, Bowlus, DA, and McGraw, RA, 1967, ASME J. Heat Transfer, 89, pp. 244–249). *J. Heat Transfer.* **1967**, *89*, 249–250. [CrossRef]
12. Malhotra, C.P.; Mahajan, R.L.; Sampath, W.S.; Barth, K.L.; Enzenroth, R.A. Control of temperature uniformity during the manufacture of stable thin-film photovoltaic devices. *Int. J. Heat Mass Transf.* **2006**, *49*, 2840–2850. [CrossRef]

13. Ahmed, N.; Dutta, M. Transient mass transfer flow past an impulsively started infinite vertical plate with ramped plate velocity and ramped temperature. *Int. J. Phys. Sci.* **2013**, *8*, 254–263.
14. Seth, G.; Hussain, S.; Sarkar, S. Hydromagnetic natural convection flow with heat and mass transfer of a chemically reacting and heat absorbing fluid past an accelerated moving vertical plate with ramped temperature and ramped surface concentration through a porous medium. *J. Egypt. Math. Soc.* **2015**, *23*, 197–207. [CrossRef]
15. Seth, G.; Sharma, R.; Sarkar, S. Natural Convection Heat and Mass Transfer Flow with Hall Current, Rotation, Radiation and Heat Absorption Past an Accelerated Moving Vertical Plate with Ramped Temperature. *J. Appl. Fluid Mech.* **2015**, *8*, 7–20.
16. Seth, G.; Sarkar, S. MHD natural convection heat and mass transfer flow past a time dependent moving vertical plate with ramped temperature in a rotating medium with Hall effects, radiation and chemical reaction. *J. Mech.* **2015**, *31*, 91–104. [CrossRef]
17. Chandran, P.; Sacheti, N.C.; Singh, A.K. Natural convection near a vertical plate with ramped wall temperature. *Heat Mass Transf.* **2005**, *41*, 459–464. [CrossRef]
18. Narahari, M.; Bég, O.A.; Ghosh, S.K. Mathematical modelling of mass transfer and free convection current effects on unsteady viscous flow with ramped wall temperature. *World J. Mech.* **2011**, *1*, 176–184. [CrossRef]
19. Khan, I. A note on exact solutions for the unsteady free convection flow of a Jeffrey fluid. *Z. Für Naturforschung A* **2015**, *70*, 397–401. [CrossRef]
20. Mohd Zin, N.A.; Khan, I.; Shafie, S. Influence of thermal radiation on unsteady MHD free convection flow of Jeffrey fluid over a vertical plate with ramped wall temperature. *Math. Probl. Eng.* **2016**, *2016*, 6257071. [CrossRef]
21. Maqbool, K.; Mann, A.; Tiwana, M. Unsteady MHD convective flow of a Jeffery fluid embedded in a porous medium with ramped wall velocity and temperature. *Alex. Eng. J.* **2018**, *57*, 1071–1078. [CrossRef]
22. Myers, J.; Bellin, D. Ramp exercise protocols for clinical and cardiopulmonary exercise testing. *Sport. Med.* **2000**, *30*, 23–29. [CrossRef]
23. Bruce, R. Evaluation of functional capacity and exercise tolerance of cardiac patients. *Mod. Concepts Cardiovasc. Dis.* **1956**, *25*, 321.
24. Hayat, T.; Siddiqui, A.M.; Asghar, S. Some simple flows of an Oldroyd-B fluid. *Int. J. Eng. Sci.* **2001**, *39*, 135–147. [CrossRef]
25. Asghar, S.; Parveen, S.; Hanif, S.; Siddiqui, A.M.; Hayat, T. Hall effects on the unsteady hydromagnetic flows of an Oldroyd-B fluid. *Int. J. Eng. Sci.* **2003**, *41*, 609–619. [CrossRef]
26. Rajagopal, K.; Ruzicka, M.; Srinivasa, A. On the Oberbeck-Boussinesq approximation. *Math. Model. Methods Appl. Sci.* **1996**, *6*, 1157–1167. [CrossRef]
27. Tiwana, M.H.; Mann, A.B.; Rizwan, M.; Maqbool, K.; Javeed, S.; Raza, S.; Khan, M.S. Unsteady Magnetohydrodynamic Convective Fluid Flow of Oldroyd-B Model Considering Ramped Wall Temperature and Ramped Wall Velocity. *Mathematics* **2019**, *7*, 676. [CrossRef]
28. Rosseland, S. *Astrophysik: Auf Atomtheoretischer Grundlage*; Springer: Berlin/Heidelberg, Germany, 2013; Volume 11.
29. Wilbur, R. Lepage. *In Complex Variables and the Laplace transform for Engineers*; McGraw Hill Book Company: New York, NY, USA, 1961.
30. Durbin, F. Numerical inversion of Laplace transforms: An efficient improvement to Dubner and Abate's method. *Comput. J.* **1974**, *17*, 371–376. [CrossRef]
31. Seth, G.; Nandkeolyar, R.; Ansari, M.S. Effect of rotation on unsteady hydromagnetic natural convection flow past an impulsively moving vertical plate with ramped temperature in a porous medium with thermal diffusion and heat absorption. *Int. J. Appl. Math. Mech.* **2011**, *7*, 52–69.
32. Khan, A.; Khan, I.; Ali, F.; Shafie, S. Effects of wall shear stress on unsteady MHD conjugate flow in a porous medium with ramped wall temperature. *PLoS ONE* **2014**, *9*, e90280. [CrossRef]



© 2020 by the authors. Licensee MDPI, Basel, Switzerland. This article is an open access article distributed under the terms and conditions of the Creative Commons Attribution (CC BY) license (http://creativecommons.org/licenses/by/4.0/).